High-order numerical solution of the nonlinear Helmholtz equation with axial symmetry

G. Baruch[a], G. Fibich[a], S. Tsynkov[b],[*],[1]

[a]*Department of Applied Mathematics, School of Mathematical Sciences, Tel Aviv University, Ramat Aviv, Tel Aviv 69978, Israel*
[b]*Department of Mathematics, North Carolina State University, Box 8205, Raleigh, NC 27695, USA*

Abstract

The nonlinear Helmholtz (NLH) equation models the propagation of intense laser beams in a Kerr medium. The NLH takes into account the effects of nonparaxiality and backward scattering that are neglected in the more common nonlinear Schrödinger model. In [G. Fibich, S. Tsynkov, High-order two-way artificial boundary conditions for nonlinear wave propagation with backscattering, J. Comput. Phys., 171 (2001) 632–677] and [G. Fibich, S. Tsynkov, Numerical solution of the nonlinear Helmholtz equation using nonorthogonal expansions, J. Comput. Phys., 210 (2005) 183–224], a novel high-order numerical method for solving the NLH was introduced and implemented in the case of a two-dimensional Cartesian geometry. The NLH was solved iteratively, using the separation of variables and a special nonlocal two-way artificial boundary condition applied to the resulting decoupled linear systems. In the current paper, we propose a major improvement to the previous method. Instead of using LU decomposition after the separation of variables, we employ an efficient summation rule that evaluates convolution with the discrete Green's function. We also extend the method to a three-dimensional setting with cylindrical symmetry, under both Dirichlet and Sommerfeld-type transverse boundary conditions.

1. Introduction

The nonlinear Helmholtz (NLH) equation

$$\Delta E(x_1, \ldots, x_D) + k_0^2(1 + \varepsilon|E|^{2\sigma})E = 0 \tag{1}$$

governs the propagation of time-harmonic electromagnetic waves in Kerr-type media. In Eq. (1), $E = E(x_1, \ldots, x_D)$ denotes the linearly polarized electric field, $\Delta = \partial_{x_1}^2 + \cdots + \partial_{x_D}^2$ is the D-dimensional Laplacian, k_0 is the linear

---

* Corresponding author. Tel.: +1 919 515 1877; fax: +1 919 513 7336.

E-mail addresses: guybar@tau.ac.il (G. Baruch), fibich@math.tau.ac.il (G. Fibich), tsynkov@math.ncsu.edu (S. Tsynkov)

URLs: http://www.tau.ac.il/~guybar (G. Baruch), http://www.math.tau.ac.il/~fibich (G. Fibich), http://www.math.ncsu.edu/~stsynkov (S. Tsynkov).
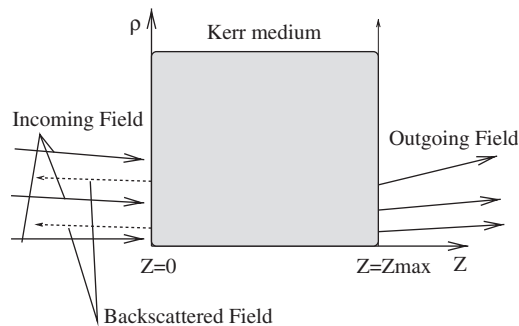
Fig. 1. Physical setup.

wavenumber and $\varepsilon = 2n_2/n_0$, where n_0 is the linear index of refraction and n_2 is the Kerr coefficient. The value of σ is equal to one for the physical Kerr effect.

A convenient physical configuration to consider, which also corresponds to typical laboratory settings, is schematically shown in Fig. 1. It is a slab of Kerr-type material located at $(x, y, z) \in R^2 \times [0, z_{\max}]$. An incoming beam impinges on the boundary $z = 0$ from the left. Most of the impinging field propagates rightwards in the z direction, undergoes a nonlinear self-focusing on its way and eventually exits the region at the right boundary $z = z_{\max}$. A small left-propagating, i.e., backscattered, field may also be induced by the Kerr nonlinearity. In a more general framework, waves may impinge on the slab of the nonlinear material both from the left and from the right.

A standard approach to the modeling of nonlinear self-focusing in Kerr-type media employs the paraxial approximation and also neglects the important phenomenon of backscattering. In doing so, the NLH (1) gets replaced by the nonlinear Schrödinger (NLS) equation [7,13,17,18]. The NLS is as an evolution equation, and it is mathematically much easier to analyze and solve compared to the NLH. There are indications, however, that disregarding the non-paraxiality may in certain cases considerably alter the mathematical properties of the solutions [3,2,6]. Besides, the NLS can only properly describe the forward propagating waves, while the backscattered waves that it neglects may also play a significant role for a range of applications.

In [8], we developed a fourth-order finite-difference method for solving the NLH (1) as a genuine boundary value problem. The overall approach in [8] was to update the nonlinear term iteratively, freezing the nonlinearity at each iteration, and then solve the resulting linear equations using the separation of variables. A key element of the algorithm of [8] was a novel nonlocal two-way artificial boundary condition (ABC) set in the direction of wave propagation. This two-way ABC provided for the reflectionless propagation of the outgoing waves while also fully transmitting the given incoming beams at the boundaries of the computational domain. Altogether, the method has enabled the direct numerical simulation of nonlinear self-focusing in the nonparaxial regime, including quantitative prediction of the important phenomenon of backscattering [5]. To the best of our knowledge, this capacity has not been achieved before in nonlinear optics. Using the methodology of [8], we also analyzed the NLH with linear damping [6], and demonstrated that for studying the key effect of critical self-focusing when $\sigma(D - 1) = 2$, this model has certain advantages over the less comprehensive NLS model, which neglects the nonparaxiality and backscattering.

An important part of the algorithm of [8] is the Dirichlet boundary conditions set in the direction orthogonal to that of the beam propagation. Although easy to implement, the transverse Dirichlet boundary conditions introduce non-physical reflections from the artificial boundary, which degrade both the numerical performance and the physical correctness of the method. In a subsequent work [9] we introduced an improved version of the algorithm of [8] that employed the Sommerfeld-type local radiation boundary conditions in the transverse direction. These conditions were constructed directly in the discrete framework for the chosen fourth-order scheme that approximates the Helmholtz operator. Numerically, implementation of the Sommerfeld conditions requires evaluation of the eigenvalues and eigenvectors of a non-Hermitian matrix. The eigenvectors are not orthogonal, yet they are linearly independent. The expansion with respect to the eigenvectors diagonalizes the transverse differentiation matrix and as such enables the separation of variables in the framework of an implicit iterative solver. It turns out that in spite of the additional effort due to the expansion with respect to a nonorthogonal basis, the algorithm of [9] offers considerable overall benefits, both from the standpoint of its numerical performance and the range of physical phenomena that it is capable of simulating.

In the current paper, we introduce a major modification to the longitudinal one-dimensional solver of the original method. This solver is applied to all decoupled systems obtained on every iteration after the separation of variables. It is a key component of the overall procedure, where the two-way BC is applied. In [8,9], the one-dimensional solver was based on discretization of the differential operator (and two-way BC) and its inversion via LU decomposition. Hereafter, we rather employ an efficient summation scheme that allows us to directly evaluate the discrete convolutions with the finite-difference Green's function. In doing so, we no longer need to explicitly construct and then invert the matrices of the fourth-order difference operators that we use. In addition, the proposed convolution-based scheme yields a noticeable improvement in numerical performance.

We also note that in all our previous work [6,8,5,9], we have only used the $2D$ Cartesian geometry. In doing so, to maintain the criticality $\sigma(D - 1) = 2$ for $D = 2$ (see [7]) we had to consider an artificial value of $\sigma = 2$. In the current paper we rather explore the actual physical case of $\sigma = 1$ and $D = 3$, which models the propagation of a laser beam in a bulk Kerr medium [12,4]. Since the computation of a true $3D$ solution is expensive we consider a cylindrically symmetric NLH:

$$\Delta_\rho E(\rho, z) + \partial_z^2 E + k_0^2(1 + \varepsilon|E|^{2\sigma})E = 0,$$

$$\Delta_\rho = \frac{1}{\rho}\partial_\rho(\rho\partial_\rho) \equiv \frac{1}{\rho}\partial_\rho + \partial_\rho^2, \tag{2}$$

where $\rho = \sqrt{x^2 + y^2}$. This allows us to study the $3D$ problem at the cost of a two-dimensional model. Cylindrical geometry brings along several major changes in the numerical procedure. First, the variable coefficients of the transverse Laplacian Δ_ρ imply that there are no closed form solutions to the corresponding homogeneous finite-difference equation. Hence, unlike the $2D$ case, the transverse radiation boundary conditions cannot be obtained directly in the discrete framework. Second, the eigenvectors of the fourth-order cylindrical Laplacian lose the orthogonality properties of their Cartesian counterparts [9], which affects the separation of variables. We expand on this phenomenon in Section 3.3.

The paper is organized as follows: In Section 2 we use a continuous formulation to describe the algorithm for solving the NLH (2). We present the nonlinear iteration scheme, the separation of variables in the cylindrically symmetric case and the two-way boundary conditions. In Section 3 we describe our fourth-order discrete formulation of the algorithm—the finite-difference scheme, the discrete separation of variables (Section 3.1) that involves building a fourth-order transverse difference Laplacian (Section 3.2) and expanding the solution with respect to its eigenvectors (Section 3.3), and the convolution based one-dimensional linear solver (Section 3.4). We corroborate our analysis by numerical validations in Sections 4.1 and 4.2, and by some typical simulations in Section 4.3. Finally, we discuss the results in Section 5.

2. Algorithm—continuous formulation

We only sketch the general scheme here and refer the reader to [8,9], where more details can be found. We solve the NLH (2) iteratively by freezing the nonlinearity and reducing the NLH to a linear variable-coefficient equation on every iteration:

$$(\Delta_\rho + \partial_z^2 + k_0^2(1 + \varepsilon|E^{(j-1)}|^{2\sigma}))E^{(j)}(\rho, z) = 0, \quad j = 1, 2, \ldots, \infty. \tag{3}$$

Eq. (3), in turn, is also addressed by iterations for every j. In doing so, we need to repeatedly solve a constant-coefficient inhomogeneous linear Helmholtz (LH) equation:

$$(\Delta_\rho + \partial_z^2 + k_0^2)E^{(j,k)} = \Phi^{(j,k)}(\rho, z), \quad k = 1, 2, \ldots, K, \tag{4}$$

where the RHS $\Phi^{(j,k)}(\rho, z) = -k_0^2\varepsilon|E^{(j-1,K)}|^{2\sigma}E^{(j,k-1)}$ and $E^{(j,0)} = E^{(j-1,K)}$.

Eq. (4) is solved on a rectangular domain $[0, \rho_{\max}] \times [0, z_{\max}]$ using the separation of variables. The latter is rendered by an expansion with respect to the eigenfunctions $\psi = \psi(\rho)$ of the transverse Laplacian:

$$\Delta_\rho \psi = -(k_\perp)^2\psi, \quad 0 < \rho < \rho_{\max}, \tag{5}$$

subject to the appropriate boundary conditions, which are boundedness at the axis $\rho = 0$ and either a Dirichlet boundary condition or a Sommerfeld-type local radiation boundary condition at the outer boundary $\rho = \rho_{\max}$.

The fundamental set of solutions for Eq. (5) consists of the Bessel functions of the first kind $J_0(k_\perp \rho)$ that are bounded at $\rho = 0$, and the Bessel functions of the second kind $N_0(k_\perp \rho)$ that are unbounded at $\rho = 0$. Since the overall solution ψ must be bounded, the eigenpairs will have the form

$$\psi_l = c_l J_0(k_\perp^l \rho), \quad \lambda_l = -(k_\perp^l)^2, \quad l = 1, \ldots, \infty. \tag{6}$$

The wavenumbers $\{k_\perp^l\}$ are determined by the boundary condition at $\rho = \rho_{max}$. Under the homogeneous Dirichlet boundary condition $\psi(\rho_{max}) = 0$ the problem is self-adjoint and the eigenvalues are real. The quantities $k_\perp^l \rho_{max}$ are obtained as roots of the Bessel function: $J_0(k_\perp \rho_{max}) = 0$. However, the Dirichlet boundary condition does not model the physical problem correctly, as it leads to spurious reflections from the artificial boundary at ρ_{max}. Therefore, following [9], we apply a transverse radiation boundary condition. To do so, we approximate the original problem outside of our region of interest, i.e., for $\rho \geqslant \rho_{max}$. Namely, we consider a simplified formulation, for which the solution $E = E^{(j,k)}$ is governed by the radial constant-coefficient Helmholtz equation:

$$\Delta_\rho E + k_0^2 E = 0, \tag{7a}$$

subject to the classical Sommerfeld radiation boundary condition at infinity:

$$E(\rho) = \mathcal{O}(\rho^{-1/2}), \quad E'(\rho) - ik_0 E(\rho) = o(\rho^{-1}) \quad \text{as } \rho \longrightarrow \infty. \tag{7b}$$

The reason for introducing approximation (7a), (7b) is two-fold. The first part is motivated by physics. Far away from the center of the propagating beam, i.e., for large ρ, the nonlinearity dies off and the equation becomes linear and homogeneous. The second part—dropping the ∂_{zz} term—means that we disregard the variation of the solution along the z-axis. This, of course, is only true for a particular class of waves that propagate normally to the boundary $\rho = \rho_{max}$, i.e., for the genuine cylindrical waves. All other waves will be partially reflected by the boundary $\rho = \rho_{max}$. As demonstrated in [9] for the Cartesian geometry, this still presents a very considerable improvement over the fully reflecting Dirichlet case.

The general solution of Eq. (7a) can be written as $E = c_1 H_0^{(1)}(k_0 \rho) + c_2 H_0^{(2)}(k_0 \rho)$, where $H_0^{(1)} = J_0 + iN_0$ and $H_0^{(2)} = J_0 - iN_0$ are the Hankel functions of the first and second kind, respectively. The Hankel function of the first kind $H_0^{(1)}$ corresponds to the expanding (i.e., outgoing) cylindrical wave that satisfies the radiation condition (7b), whereas the Hankel function of the second kind $H_0^{(2)}$ corresponds to the contracting (i.e., incoming) cylindrical wave that does not satisfy (7b). We can therefore conclude that if the overall solution E were to satisfy Eq. (4) for $\rho < \rho_{max}$ and Eqs. (7a), (7b) for $\rho \geqslant \rho_{max}$, then on the exterior region $\rho \geqslant \rho_{max}$ it must have the form $E = c_1 H_0^{(1)}(k_0 \rho)$, i.e., $c_2 = 0$.

Selecting only one element $H_0^{(1)}$ out of the fundamental set $\{H_0^{(1)}, H_0^{(2)}\}$ is equivalent to requiring that the following Wronskian vanishes at ρ_{max}:

$$W(\rho_{max}) = \det \begin{bmatrix} E(\rho) & H_0^{(1)}(k_0 \rho) \\ \dfrac{d}{d\rho} E(\rho) & \dfrac{d}{d\rho} H_0^{(1)}(k_0 \rho) \end{bmatrix} \Bigg|_{\rho = \rho_{max}} = 0,$$

which immediately yields

$$\frac{\partial E}{\partial \rho} - \alpha E \Bigg|_{\rho = \rho_{max}} = 0 \quad \text{where } \alpha = \frac{(d/d\rho) H_0^{(1)}(k_0 \rho_{max})}{H_0^{(1)}(k_0 \rho_{max})} = \frac{-k_0 H_1^{(1)}(k_0 \rho_{max})}{H_0^{(1)}(k_0 \rho_{max})}. \tag{8}$$

Note that we have re-introduced the partial derivative $\partial E/\partial \rho$ in formula (8) because generally $E = E(\rho, z)$, and the boundary condition is to be set at every z.

The local radiation boundary condition (8) set at a finite location $\rho = \rho_{max}$ is obviously not identical to the Sommerfeld condition (7b) set at infinity. As, however, we have shown, boundary condition (8) is equivalent to (7b). This, in particular, indicates that if we were to try and set the actual Sommerfeld condition (7b) at a finite location rather than at infinity,[2] then we would have generated an undesired small component of the incoming wave $H_0^{(2)}(k_0 \rho)$ at $\rho = \rho_{max}$. On the other hand, the radiation condition (8) makes the artificial boundary completely transparent to all expanding cylindrical

---

[2] An approach adopted in some early studies on ABCs, see [19].

waves traveling with the fixed wavenumber k_0. Note that the boundary conditions similar to (8) have been implemented in [11] for a more elaborate setting that did not involve the axial symmetry and rather required a Fourier transform in the spherical or polar coordinates.

Applying the boundary condition (8) to the eigenfunction ψ_l of (6) we obtain an equation that determines $\{k_\perp^l\}_{l=1}^\infty$:

$$\alpha J_0(k_\perp \rho_{\max}) - k_\perp J_0'(k_\perp \rho_{\max}) = \alpha J_0(k_\perp \rho_{\max}) + k_\perp J_1(k_\perp \rho_{\max}) = 0. \tag{9}$$

Because of the radiation boundary condition, the problem is not self-adjoint. As such, the corresponding eigenvalues are generally speaking complex.

Having solved the eigenvalue problem (5), we can expand the field E and the RHS Φ with respect to the resulting system of eigenfunctions:

$$E(\rho, z) = \sum_{l=1}^\infty u_l(z)\psi_l(\rho), \quad \Phi(\rho, z) = \sum_{l=1}^\infty f_l(z)\psi_l(\rho). \tag{10}$$

Likewise, we expand the transverse profiles of the incoming waves at $z = 0$ and $z = z_{\max}$:

$$E_{\text{inc}}^{\text{left}}(\rho) = \sum_{l=1}^\infty u_{\text{inc}}^{\text{left},l}\psi_l(\rho), \quad E_{\text{inc}}^{\text{right}}(\rho) = \sum_{l=1}^\infty u_{\text{inc}}^{\text{right},l}\psi_l(\rho). \tag{11}$$

In the Dirichlet case, series (10) and (11) converge because the eigenfunctions ψ_l are known to form a complete orthonormal system in $L_2[0, \rho_{\max}]$ with the weight ρ. When the radiation condition (8) is specified at $\rho = \rho_{\max}$, the eigenfunctions have the so-called "real orthogonality" property $\int_0^{\rho_{\max}} \rho\psi_l\psi_k \, d\rho = \delta_{lk}$, see [9]. Completeness of this system of eigenfunctions can also be shown, see [1].

Decomposition (10) transforms the cylindrical linear Helmholtz equation (4) into an uncoupled system of one-dimensional Helmholtz equations with respect to $u_l(z)$:

$$\left(\frac{d^2}{dz^2} + (k_\parallel^l)^2\right)u_l(z) = f_l(z),$$

$$(k_\parallel^l)^2 = k_0^2 - (k_\perp^l)^2, \quad l = 1, 2, \ldots, \infty. \tag{12}$$

The fundamental set of solutions for each equation (12) consists of a forward propagating wave $e^{ik_\parallel^l x}$ and a backward propagating wave $e^{-ik_\parallel^l z}$. To actually solve Eqs. (12), one needs to set the boundary conditions at $z = 0$ and $z = z_{\max}$. Those will be the two-way ABCs that prescribe the incoming radiation entering the domain, and allow *the scattered waves*, i.e., the radiation generated by the nonlinear sources inside the domain, to leave it with no reflection from the artificial boundary. As discussed in [8,9], the ABCs in the longitudinal direction are a key element of the overall method. We emphasize that the two-way ABCs are defined in the transformed space individually for each transverse eigenmode l of (12), and are therefore non-local in the original space.

Definition 1. The first-order linear homogeneous differential relations

$$(\partial_z + ik_\parallel^l)u_l|_{z=0} = 0 \quad \text{and} \quad (\partial_z - ik_\parallel^l)u_l|_{z=z_{\max}} = 0 \tag{13}$$

are called the radiation boundary conditions for Eqs. (12).

Indeed, for every l the second-order differential operator of (12) can be factored into a product of two first-order operators that correspond precisely to (13):

$$\frac{d^2}{dz^2} + (k_\parallel^l)^2\boldsymbol{I} = \left(\frac{d}{dz} + ik_\parallel^l\boldsymbol{I}\right)\left(\frac{d}{dz} - ik_\parallel^l\boldsymbol{I}\right). \tag{14}$$

The first factor on the right-hand side of (14) allows the left-traveling waves $e^{-ik_\parallel^l z}$ and prohibits the right-traveling waves $e^{ik_\parallel^l z}$. The second factor on the right-hand side of (14) does exactly the opposite. We therefore conclude that

once applied to the differential equation of (12) for a given l, the boundary conditions (13) will only allow the radiation of waves due to the sources $f_l(z)$ outward from the domain $[0, z_{\max}]$. It is also easy to see that when there are no sources, $f_l(z) \equiv 0$, problem (12), (13) may only have a trivial solution: $u_l(z) = 0$. Consequently, the solvability of the inhomogeneous problem (12), (13) follows by a Fredholm-type argument.

Definition 2. Solution to the boundary value problem (12), (13) will be called the scattered field component u_{scat}.

In the context of physics, this scattered field is induced by the Kerr nonlinearity concentrated on the interval $[0, z_{\max}]$. One can easily write down the scattered field in the form of a convolution with the one-dimensional free-space Green's function

$$G(s) = \frac{1}{2ik_\parallel} e^{ik_\parallel |s|}, \tag{15}$$

which yields

$$u_{\text{scat}}(z) = \frac{1}{2ik_\parallel} \int_0^{z_{\max}} f(\zeta) e^{ik_\parallel |\zeta - z|} \, d\zeta. \tag{16}$$

Next, for a given l, consider an incoming wave in the form

$$u_{\text{inc}}^{\text{left}}(z) = u_{\text{inc}}^{\text{left},l} e^{ik_\parallel^l z}.$$

This wave propagates from the left to the right, and at the interface $z = 0$, where it enters the domain, we have $u_{\text{inc}}^{\text{left}}(0) = u_{\text{inc}}^{\text{left},l}$, see formula (11). The function $u_{\text{inc}}^{\text{left}}(z)$ also satisfies the homogeneous version of the differential equation of (12), as well as the second boundary condition of (13). Once substituted into the first boundary condition of (13), the wave $u_{\text{inc}}^{\text{left}}(z)$ generates a particular inhomogeneity:

$$(\partial_z + ik_\parallel^l) u_{\text{inc}}^{\text{left}}(z)|_{z=0} = 2ik_\parallel^l u_{\text{inc}}^{\text{left},l}.$$

Similarly, for the right traveling incoming wave

$$u_{\text{inc}}^{\text{right}}(z) = u_{\text{inc}}^{\text{right},l} e^{ik_\parallel^l (z_{\max} - z)},$$

we have

$$(\partial_z - ik_\parallel^l) u_{\text{inc}}^{\text{right}}(z)|_{z=z_{\max}} = -2ik_\parallel^l u_{\text{inc}}^{\text{right},l},$$

while otherwise the homogeneous differential equation and the first boundary condition of (13) are satisfied.

Definition 3. The first-order linear inhomogeneous differential relations

$$(\partial_z + ik_\parallel^l) u_l|_{z=0} = 2ik_\parallel^l u_{\text{inc}}^{\text{left},l},$$

$$(\partial_z - ik_\parallel^l) u_l|_{z=z_{\max}} = -2ik_\parallel^l u_{\text{inc}}^{\text{right},l}, \tag{17}$$

where $u_{\text{inc}}^{\text{left},l}$ and $u_{\text{inc}}^{\text{right},l}$ are defined in (11), are called the two-way boundary conditions for the one-dimensional Helmholtz equation (12).

Using the superposition principle, one can easily see that the solution to problem (12), (17) can be represented as a sum of the foregoing three field components:

$$u_l(z) = u_{\text{scat}}(z) + u_{\text{inc}}^{\text{left}}(z) + u_{\text{inc}}^{\text{right}}(z). \tag{18}$$

This solution is unique. One can also show that problem (12), (17) is well posed.

In our previous work [8,9], we discretized problem (12), (17) and solved numerically the resulting system of linear algebraic equations. A key part of the discretization consisted of building discrete counterparts to the boundary

conditions (17). The key improvement that we propose hereafter (see Section 3.4) is to implement an efficient discrete analogue of the convolution (16), and obtain the solution in the form (18). As we shall see in Sections 3.4 and 4.4, using the integral formulation (16) turns out to be more efficient than the differential formulation (12).

3. Algorithm—fourth-order finite difference formulation

The NLH (2) is approximated on the uniform two-dimensional grid

$$\rho_m = \left(m - \frac{1}{2}\right) h_\rho, \quad m = 1, \ldots, M, \quad h_\rho = \frac{\rho_{\max}}{M},$$

$$z_n = n h_z, \quad n = 0, \ldots, N, \quad h_z = \frac{z_{\max}}{N}. \tag{19}$$

We use a fourth-order central difference scheme that can be written as

$$L_\rho E^{(j,k)} + E^{(j,k)} L_z^{\mathrm{T}} + k_0^2 E^{(j,k)} = \Phi^{(j,k)}. \tag{20}$$

Here the $M \times (N+1)$ matrices $E_{m,n}^{(j,k)}$ and $\Phi_{m,n}^{(j,k)} = -k_0^2 \varepsilon |E_{m,n}^{(j-1,K)}|^2 E_{m,n}^{(j,k-1)}$ are the discretized field and the discretized RHS, see formulae (3) and (4), the $M \times M$ matrix L_ρ is the discrete approximation of the transverse Laplacian Δ_ρ with the appropriate boundary conditions to be introduced in Section 3.2, the symmetric $(N+1) \times (N+1)$ matrix L_z represents the discrete approximation to the second derivative ∂_z^2 and the superscript T denotes the transpose.

3.1. Separation of variables

The separation of variables consists of three stages. First, we diagonalize the transverse Laplacian L_ρ by solving the discrete eigenvalue problem

$$L_\rho \Psi = -\Psi \Lambda, \quad \Lambda = \begin{bmatrix} (k_\perp^1)^2 & & \\ & \ddots & \\ & & (k_\perp^M)^2 \end{bmatrix}. \tag{21}$$

Second, we expand the field E and the RHS Φ with respect to the basis composed of the eigenvectors of L_ρ:

$$E = \Psi U, \quad \Phi = \Psi F. \tag{22}$$

Third, we substitute (22) into the discretized LH (20)

$$L_\rho \Psi U + \Psi U L_z^{\mathrm{T}} + k_0^2 \Psi U = \Psi(k_0^2 I_M - \Lambda)U + \Psi U L_z^{\mathrm{T}} = \Psi F$$

to obtain

$$L_z U^{\mathrm{T}} + U^{\mathrm{T}}(k_0^2 I_M - \Lambda) = F^{\mathrm{T}}.$$

This equation is a collection of decoupled one-dimensional linear Helmholtz equations for each column of U^{T}:

$$\frac{-u_{l,n-2} + 16u_{l,n-1} - 30u_{l,n} + 16u_{l,n+1} - u_{l,n+2}}{12h_z^2} + (k_\parallel^l)^2 u_{l,n} = f_{l,n},$$

$$(k_\parallel^l)^2 = k_0^2 - (k_\perp^l)^2, \quad l = 1, \ldots, M. \tag{23}$$

In formula (23), $u_{l,n}$ and $f_{l,n}$ denote entries of the matrices U and F, respectively.

The overall solution procedure can be summarized by the following algorithm:

Agorithm 1. *Solution of Eq.* (4) *using the discrete separation of variables.*
   Preprocessing:
   (0.1) *Solve the eigenvalue problem* (21) *with* L_ρ *as defined in Section* 3.2 *to obtain the matrix of eigenvectors* Ψ.
   (0.2) *Perform the LU decomposition of* Ψ.
   (0.3) *Obtain the transformations of the incoming fields* $u_{\text{inc}}^{\text{left}} = \Psi^{-1} E_{\text{inc}}^{\text{left}}$ *and* $u_{\text{inc}}^{\text{right}} = \Psi^{-1} E_{\text{inc}}^{\text{right}}$.

   At every iteration of (3), (4):
   (1) *Build the RHS matrix* Φ.
   (2) *Obtain F by the transformation* $F = \Psi^{-1}\Phi$.
   (3) *For each eigenmode l, solve Eq.* (23) *using the method of Section* 3.4.
   (4) *Evaluate the field E by transforming back*: $E = \Psi U$.

The implementation of transformations (22) is considered in Section 3.3.

3.2. Approximation of the transverse Laplacian

The operator Δ_ρ is discretized by the fourth-order central differences:

$$L_\rho u|_{\rho=\rho_m} = \frac{-u_{m-2} + 16u_{m-1} - 30u_m + 16u_{m+1} - u_{m+2}}{12h_\rho^2}$$

$$+ \frac{1}{\rho_m} \cdot \frac{u_{m-2} - 8u_{m-1} + 8u_{m+1} - u_{m+2}}{12h_\rho}. \tag{24}$$

In the matrix form we can use (19) for ρ_m and write

$$L_\rho = \frac{1}{12h_\rho^2}
\begin{bmatrix}
L_{11} & L_{12} & -3 & & & \\
L_{21} & L_{22} & 16 \cdot \frac{4}{3} & -\frac{5}{3} & & \\
\ddots & \ddots & \ddots & \ddots & \ddots & \\
-\dfrac{m-\frac{3}{2}}{m-\frac{1}{2}} & 16\dfrac{m-1}{m-\frac{1}{2}} & -30 & 16\dfrac{m}{m-\frac{1}{2}} & -\dfrac{m+\frac{1}{2}}{m-\frac{1}{2}} & \\
& \ddots & \ddots & \ddots & \ddots & \ddots \\
& & -\dfrac{M-\frac{5}{2}}{M-\frac{3}{2}} & L_{M-1,M-2} & L_{M-1,M-1} & L_{M-1,M} \\
& & & L_{M,M-2} & L_{M,M-1} & L_{M,M}
\end{bmatrix}, \tag{25}$$

where the first two rows and the last two rows are modified to account for the transverse boundary conditions. To actually obtain these modified rows, we introduce a pair of ghost nodes beyond each boundary: $\{u_{-1}, u_0\}$ and $\{u_{M+1}, u_{M+2}\}$, which will eventually be eliminated.

Axial symmetry, along with the requirement of boundedness at $\rho = 0$, implies that the grid function u_m must be even. Hence, using the definition of grid (19), we have $u_0 = u(-h_\rho/2) = u(h_\rho/2) = u_1$ and similarly $u_{-1} = u_2$. Consequently, the fourth-order approximation of Δ_ρ at ρ_1 becomes $(-30u_1 + 33u_2 - 3u_3)/12h^2$ and at ρ_2 it is $(31u_1 - 90u_2 + 64u_3 - 5u_4)/36h^2$. Combining these two relations we obtain

$$L_{1:2,1:2} = \begin{bmatrix} -30 & 33 \\ \dfrac{31}{3} & -30 \end{bmatrix}. \tag{26}$$

At the outer boundary $\rho = \rho_{max}$, two conditions are needed because the approximation is fourth-order. The first one is determined by the physical requirement; it may be either a Dirichlet or a radiation condition. The choice of the second condition allows more flexibility as long as the resulting method is fourth-order and stable.[3] Hereafter, this second condition is to let the ghost value u_{M+2} be equal to the fourth-order extrapolation of $\{u_{M-2}, \ldots, u_{M+1}\}$, which can be conveniently written as

$$u_{M+2} = \sum_{j=-2}^{1} (-1)^{1+j} \binom{4}{2-j} u_{M+j}. \tag{27}$$

As for the (first) physical boundary condition, we first represent it as a general homogeneous relation of the type $[c_{-2}, \ldots, c_2][u_{M-2}, \ldots, u_{M+2}]^T = 0$, and then use it to build the block $L_{M-1:M, M-2:M}$ of matrix (25). A fourth-order approximation of the Dirichlet boundary condition at $\rho = \rho_{M+1/2} = \rho_{max}$ can be written as

$$u_{M+1/2} \approx \frac{-u_{M-1} + 9u_M + 9u_{M+1} - u_{M+2}}{16} = 0.$$

Therefore,

$$c_{-2:2}^D = [0, -1, 9, 9, -1]. \tag{28}$$

Similarly, a fourth-order approximation of the Sommerfeld-type radiation boundary condition (8) at $\rho_{M+1/2}$ can be written as

$$\frac{u_{M-1} - 27u_M + 27u_{M+1} - u_{M+2}}{48h_\rho/2} = \alpha \frac{-u_{M-1} + 9u_M + 9u_{M+1} - u_{M+2}}{16},$$

which implies

$$c_{-2:2}^S = [0, 1, -27, 27, -1] - \tfrac{3}{2}\alpha h_\rho[0, -1, 9, 9, -1]. \tag{29}$$

Combining either of relations (28) or (29) with (27) into

$$\begin{bmatrix} c_{-2} & c_{-1} & c_0 & c_1 & c_2 \\ -1 & 4 & -6 & 4 & -1 \end{bmatrix} \begin{bmatrix} u_{M-2} \\ \vdots \\ u_{M+2} \end{bmatrix} = \begin{bmatrix} 0 \\ 0 \end{bmatrix},$$

we can express the ghost values u_{M+1} and u_{M+2} in terms of the interior values

$$u_{M+i} = \vec{v}_i \cdot \begin{bmatrix} u_{M-2} \\ u_{M-1} \\ u_M \end{bmatrix}, \quad i = 1, 2, \tag{30}$$

where

$$\vec{v}_1 = -\begin{bmatrix} \dfrac{c_{-2} - c_2}{c_1 + 4c_2} & \dfrac{c_{-1} + 4c_2}{c_1 + 4c_2} & \dfrac{c_0 - 6c_2}{c_1 + 4c_2} \end{bmatrix}, \quad \vec{v}_2 = -\begin{bmatrix} \dfrac{4c_{-2} + c_1}{c_1 + 4c_2} & \dfrac{4c_{-1} - 4c_1}{c_1 + 4c_2} & \dfrac{4c_0 + 6c_1}{c_1 + 4c_2} \end{bmatrix}.$$

Finally, we substitute expressions (30) into formula (24) for ρ_{M-1} and ρ_M, to obtain

$$L_{M-1:M, M-2:M} = \begin{bmatrix} 16\dfrac{M-2}{M-\frac{3}{2}} & -30 & 16\dfrac{M-1}{M-\frac{3}{2}} \\ -\dfrac{M-\frac{3}{2}}{M-\frac{1}{2}} & 16\dfrac{M-1}{M-\frac{1}{2}} & -30 \end{bmatrix} + \begin{bmatrix} -\dfrac{M-\frac{1}{2}}{M-\frac{3}{2}}\vec{v}_1 \\ \dfrac{16M}{M-\frac{1}{2}}\vec{v}_1 - \dfrac{M+\frac{1}{2}}{M-\frac{1}{2}}\vec{v}_2 \end{bmatrix}.$$

---

[3] Stability of the approximations of this type can be studied by the methodology of [14].

3.3. Expansion with respect to the eigenvectors

Having defined and solved the discrete eigenvalue problem (21), let us now consider the implementation of the transformations $\Phi \to F$ and $U \to E$ performed in Algorithm 1. These transformations, defined by formulae (22), are the discrete counterparts of expansions (10).

For the Cartesian case with the Dirichlet boundary conditions [8], the discrete transverse Laplacian is self-adjoint and its eigenvectors form an orthonormal basis. These eigenvectors are given by the trigonometric functions on the grid. Accordingly, the transformations rendered by Ψ and Ψ^{-1} are the discrete Fourier transforms that can be implemented efficiently using FFT at a cost of $\mathcal{O}(N \cdot M \log M)$ operations per transformation.

For the Cartesian case with the radiation boundary condition [9], the transverse Laplacian is no longer self-adjoint. Its eigenvectors are not orthogonal in the true sense of the word, although they are linearly independent. We are not aware of a fast algorithm (similar to FFT) for computing the expansion with respect to these eigenvectors. As such, the transformations are implemented at a cost of $\mathcal{O}(N \cdot M^2)$ operations each. As shown in [9], however, this case is characterized by the real orthogonality property of the eigenvectors. This still brings along an additional advantage compared to the completely generic case, because the inversion of the matrix Ψ [Step (0.2) in Algorithm 1] reduces to taking its transpose.

For the current axially symmetric case, the latter advantage is lost. The fourth order discrete Laplacian is non-self-adjoint not only for the Sommerfeld boundary conditions but even when the Dirichlet boundary conditions are set at $\rho = \rho_{\max}$. The reason is that the block $\begin{bmatrix} L_{11} & L_{12} \\ L_{21} & L_{22} \end{bmatrix}$ of matrix (25), see formula (26), is non-symmetric with respect to the appropriate weighted inner product (with the weight ρ). As a result, the eigenvectors are neither orthogonal nor real orthogonal, and the transformation $F = \Psi^{-1}\Phi$ must be carried out using the LU factorization of the matrix Ψ, adding an $\mathcal{O}(M^3)$ preprocessing cost [Step (0.2) in Algorithm 1].

At the current moment of time, we do not have a full understanding yet of the loss of real orthogonality in the fourth-order case. We note that the second-order central difference cylindrical Laplacian keeps the appropriate weighted symmetry near $\rho = 0$ and as such its eigenvectors remain real orthogonal. The loss of this property in the fourth-order case may be pertinent to the specific discretization used, and another fourth-order discretization can possibly be found in the future that will have real orthogonal eigenvectors. Of course, this may prove tedious. As, for example, shown in [16], keeping symmetry and higher order depends on the details of the approximation, and in the case of the cylindrical coordinates it may be particularly hard.

On the other hand, apart from the somewhat increased computational cost, the loss of real orthogonality in the fourth-order cylindrical case does not seem to inflict any other negative implications. We emphasize that the actual orthogonality is lost anyway because of the Sommerfeld boundary conditions that represent the correct physics. This loss would have hampered the performance in any event (in both the cylindrical and Cartesian cases) if we were to use an iterative solver to invert the constant coefficient operator. As, however, we are using a direct solver based on the separation of variables, this issue is less crucial.

An alternative option to explore in the future may be the use of compact nine point stencils instead of the extended five point differences in each direction, see, e.g., [10,15]. It is, however, unclear whether or not it will be possible to find one and the same diagonalizing transformation for all three transverse one-dimensional sub-stencils of the 3×3 stencil. If this is not the case, then the separation of variables cannot be performed, and the nonlocal two-way ABCs in the direction of propagation cannot be set.

3.4. Fast solution of Eq. (23) using discrete convolutions

To solve Eq. (23) subject to the two-way boundary conditions, we introduce a new approach in this paper that differs fundamentally from that of [8,9]. It is based on the direct evaluation of discrete convolutions with the finite-difference Green's function. The new algorithm does not require building difference analogues to boundary conditions (17). It also offers a considerably better numerical performance compared to the original approach based on the explicit construction and inversion of the difference operator L_z. Yet the new technique remains mathematically equivalent to the original one.

In [8], we have explicitly obtained the finite-difference counterparts to the radiation boundary conditions (13) and to the two-way boundary conditions (17). It was shown in [8] that the solution u_{scat} of Eq. (23) subject to the

finite-difference radiation boundary conditions of [8] can be written as the discrete convolution

$$u_n = \sum_{j=0}^{N} f_j G^{n-j} \tag{31}$$

of the sources f_n with the finite-difference Green's function

$$G^n = \sum_{i=1,2} a_i q_i^{|n|} = \sum_{\substack{i=1,2 \\ \sigma=\pm 1}} \Theta_{\sigma n} a_i q_i^{\sigma n} - \delta_n (a_1 + a_2). \tag{32}$$

In formula (32),

$$\Theta_n = \begin{cases} 1, & n \geqslant 0 \\ 0, & n < 0 \end{cases} \quad \text{and} \quad \delta_n = \begin{cases} 1, & n = 0, \\ 0, & n \neq 0 \end{cases}$$

are the discrete Heaviside function and the discrete Kronecker delta function, respectively. The quantities a_i and q_i, $i = 1, 2$, in formula (32) are defined in [8].[4] It was also shown in [8] that $q_1 \approx e^{ik_\parallel h_z}$. Consequently, the contributions of the $i = 1$ terms to the finite-difference Green's function (32) and to the discrete convolution (31) are analogous to the full continuous Green's function (15) and the continuous convolution (16), respectively. The $i = 2$ terms are the non-physical evanescent waves $q_2^{|n-j|}$ that appear in the discrete solution because the approximation is fourth-order, whereas the original differential equation is only second-order.

A straightforward evaluation of the convolution (31) for $n = 0, \ldots, N$ costs $\mathcal{O}(N^2)$ arithmetic operations. This perceived cost led in [8] to the use of the LU factorization for solving Eq. (23), which has an $\mathcal{O}(N)$ cost. The actual formulation (31), which is based on Green's function, was only used in [8,9] as an analytical tool to derive the discrete two-way boundary conditions, but was never employed for simulations.

We now present an $\mathcal{O}(N)$ algorithm for the direct calculation of convolution (31). It allows us to solve Eq. (23) subject to the discrete two-way boundary conditions analogous to (17).

Substitution of expression (32) into formula (31) yields

$$u_n + f_n (a_1 + a_2) = \sum_{j=0}^{N} f_m \sum_{\substack{i=1,2 \\ \sigma=\pm 1}} \Theta_{\sigma(n-j)} a_i q_i^{\sigma(n-j)}$$

$$= \sum_{\substack{i=1,2 \\ \sigma=\pm 1}} a_i \sum_{j=0}^{N} f_j \Theta_{\sigma(n-j)} q_i^{\sigma(n-j)} = \sum_{\substack{i=1,2 \\ \sigma=\pm 1}} a_i H_{i,\sigma}^n, \tag{33}$$

where the partial convolutions

$$H_{i,\sigma}^n = \sum_{j=0}^{N} \Theta_{\sigma(n-j)} f_j q_i^{\sigma(n-j)}$$

are contributions of the forward and backward propagating discrete waves $q_i^{\pm m}$ to the overall sum (31). Since for $\sigma = +1$ and $\sigma = -1$ we have

$$H_{i,+}^n = \sum_{j=0}^{n} f_j q_i^{(n-j)} \quad \text{and} \quad H_{i,-}^n = \sum_{j=n}^{N} f_j q_i^{-(n-j)},$$

we can derive the following recursion relations:

$$H_{i,+}^n = q_i H_{i,+}^{n-1} + f_n \quad \text{and} \quad H_{i,-}^n = q_i H_{i,-}^{n+1} + f_n \tag{34}$$

---

[4] In fact, four coefficients are given in [8]: a_1 and a_2 for $n > 0$ and b_1 and b_2 for $n < 0$. However, Green's function is symmetric with respect to $n = 0$, and $a_i = b_i$.

Table 1
The error $\|E^{(h)} - E\|_\infty$ in the linear case

(h_ρ, h_z)	$\left(\frac{\lambda_0}{2}, \frac{\lambda_0}{10}\right)$	$\left(\frac{\lambda_0}{4}, \frac{\lambda_0}{20}\right)$	$\left(\frac{\lambda_0}{8}, \frac{\lambda_0}{40}\right)$	$\left(\frac{\lambda_0}{16}, \frac{\lambda_0}{80}\right)$
Error	0.26	0.016	0.0011	0.000076

that admit an intuitive physical interpretation: the induced monochromatic electric field at location z is the field induced on $z \pm h_z$ times a phase factor q_i, plus the field induced by the sources f_n in the interval $(z - h_z/2, z + h_z/2)$.

The recursive formulae (34) yield $H_{i,\pm}^n$ for all $n = 0, \ldots, N$ together at an $\mathcal{O}(N)$ cost. The overall algorithm can therefore be implemented as follows:

Agorithm 2. *Solution of Eq.* (23) *using the discrete Green's function*:
  (1) *for* $n = N, \ldots, 0$ *calculate* $H_{i,-}^n$ *with the help of* (34);
  (2) *for* $n = 0, \ldots, N$ *calculate* $H_{i,+}^n$ *with the help of* (34);
  (3) *for* $n = 0, \ldots, N$ *calculate* u_n *with the help of* (33).

Algorithm 2 provides the scattered component u_{scat} of the discrete solution. The incoming radiation components $u_{\text{inc}}^{\text{left}} q_1^n$ and $u_{\text{inc}}^{\text{right}} q_1^{N-n}$ are simply added as in (18).

Computational benefits associated with using this method compared to our previous method [8,9] are outlined in Section 4.4.

4. Numerical demonstrations

4.1. Linear Helmholtz equation

To assess the numerical performance of the linear Helmholtz solver, we first solve a model problem with variable coefficients, for which the exact solution can be explicitly obtained. The setting is similar to that of [8, Section 7.1], and consists of a superposition of a right-traveling wave E_{right} and a left-traveling wave E_{left}. Specifically, we will solve the linear Helmholtz equation

$$(\Delta + k^2(z))E(\rho, z) = 0$$

subject to the transverse radiation boundary condition, and with the incoming wave $E_{\text{inc}}^{\text{left}} = e^{ik_\parallel^l z} J_0(k_\perp^l \rho)$. The functions $k(z)$ and $E_{\text{inc}}^{\text{left}}$ were chosen (see [8, Section 7.1] for detail) so that the analytic solution be given by $E = E_{\text{right}} + \frac{1}{2}E_{\text{left}}$, where

$$E_{\text{right}} = e^{ik_\parallel^l z} J_0(k_\perp^l \rho)[1 + 0.2 \cdot z^4 e^{-z}],$$

$$E_{\text{left}} = e^{-ik_\parallel^l z} J_0(k_\perp^l \rho)[1 + e^{-(z/3)^2}].$$

Here $k_\perp^l$ is the complex-valued wavenumber that satisfies equality (9). The parameters used are $k_0 = 2\pi/\lambda_0 = 20$, $k_\perp^l = k_\perp^5 \approx (14.92 - 0.392i)/\rho_{\max}$, $z_{\max} = 30$ and $\rho_{\max} = 2$. The deviation of the computed field $E^{(h)}$ from the analytic exact solution E is given in Table 1, and shows the expected fourth-order convergence.

4.2. Nonlinear Helmholtz equation

We solve the NLH (2) for $\sigma = 1$, $k_0 = 2\pi/\lambda_0 = 8$, and with a Gaussian incoming beam $E_{\text{inc}}^{\text{left}}(\rho) = e^{-\rho^2}$. The parameter that controls the beam collapse in the corresponding critical NLS $i\psi_z + \Delta_\perp \psi + |\psi|^2 \psi = 0$ is the ratio of the incoming beam power $N_0 = \int_0^\infty \rho e^{-2\rho^2} \, d\rho = \frac{1}{4}$ to the critical power $N_c \approx 1.8623$ [7]. For the NLH (2), this power ratio p
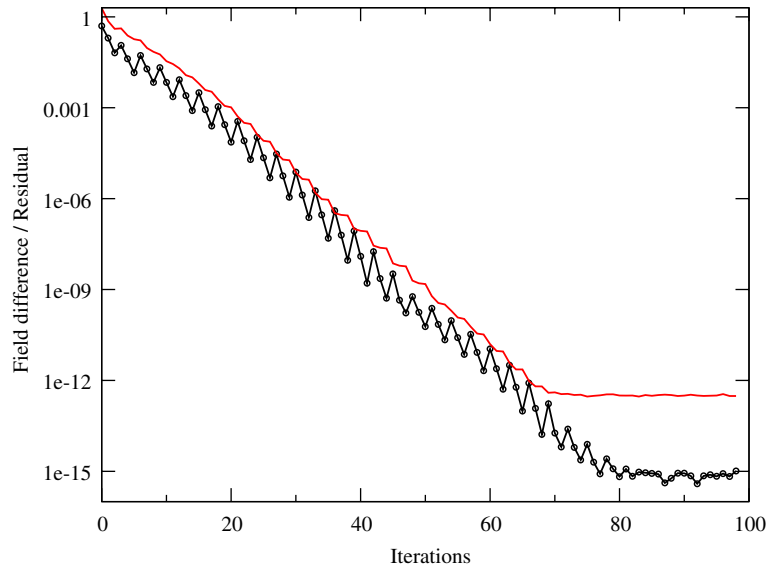
Fig. 2. Inter-iteration difference $\|E^j - E^{j-1}\|_\infty$ (solid) and residual $\|R\|_\infty$ (dots) over 33 nonlinear iterations with $K = 3$ inner-loop iterations.

Table 2
Grid refinement study for $p = 0.7$, $\rho_{\max} = 10$, $z_{\max} = 30$, and with radiation BC

(h_ρ, h_z)	$\left(\frac{\lambda_0}{2}, \frac{\lambda_0}{5}\right)$	$\left(\frac{\lambda_0}{4}, \frac{\lambda_0}{10}\right)$	$\left(\frac{\lambda_0}{8}, \frac{\lambda_0}{20}\right)$	$\left(\frac{\lambda_0}{16}, \frac{\lambda_0}{40}\right)$	$\left(\frac{\lambda_0}{32}, \frac{\lambda_0}{80}\right)$
$\|E^{(2h)} - E^{(h)}\|_\infty$		0.59	0.049	0.0044	0.0017

is related to the nonlinearity coefficient ε via

$$p = \frac{N_0}{N_c} \approx \frac{k_0^2 \varepsilon}{4 \cdot 1.8623}.$$

In order to quantify the convergence of the iterations, both the inter-iteration difference in the field $\|E^{(j)} - E^{(j+1)}\|_\infty = \max_{m,n} |E_{m,n}^{(i)} - E_{m,n}^{(i+1)}|$ and the maximum residual $\|R\|_\infty$ were monitored, where the residual is defined as $R = L_\rho E + E L_z^T + (k_0^2 + \varepsilon |E_{mn}|^2)E$, see Eq. (20). The results of a typical run, with moderate nonlinearity $p = 0.7$ and with radiation transverse boundary condition, are displayed in Fig. 2. Fig. 2 shows that the convergence history of the new algorithm is very similar to that of the previous algorithms of [8,9]. The residual decreases by 12 orders of magnitude, while the inter-iteration difference decreases to machine accuracy $\sim 10^{-16}$.

In order to demonstrate the fourth-order grid convergence in the nonlinear regime, we synchronously refine the grid in both the transverse and the longitudinal directions. In doing so, we monitor the maximum difference between the fields on each two consecutive grids (the coarser and the finer). The results are displayed in Table 2. For low resolutions, the convergence rate is $\mathcal{O}(h^{3.5})$, which is close to the theoretical $\mathcal{O}(h^4)$. However, at high resolutions $(h_\rho, h_z) \lesssim (\lambda_0/20, \lambda_0/80)$ that were not included in the previous studies due to the lack of resources, we observe a certain deterioration of the rate of grid convergence. The mechanisms of this deterioration are under current research.

4.3. A typical simulation

We first present the case of a Gaussian input beam with $p = 0.7$. The numerical parameters used are $k_0 = 8$, $h_z = \lambda_0/100$, $h_\rho = \lambda_0/20$, $z_{\max} = 30$ and $\rho_{\max} = 10$. The on-axis amplitude of the field $|E(0, z)|$ is displayed in Fig. 3A. It exhibits a moderate self-focusing followed by the ultimate diffraction, in agreement with the predictions of the simplified NLS model for a beam whose power is below the critical threshold ($p = 1$) for the collapse. Furthermore, solution with the
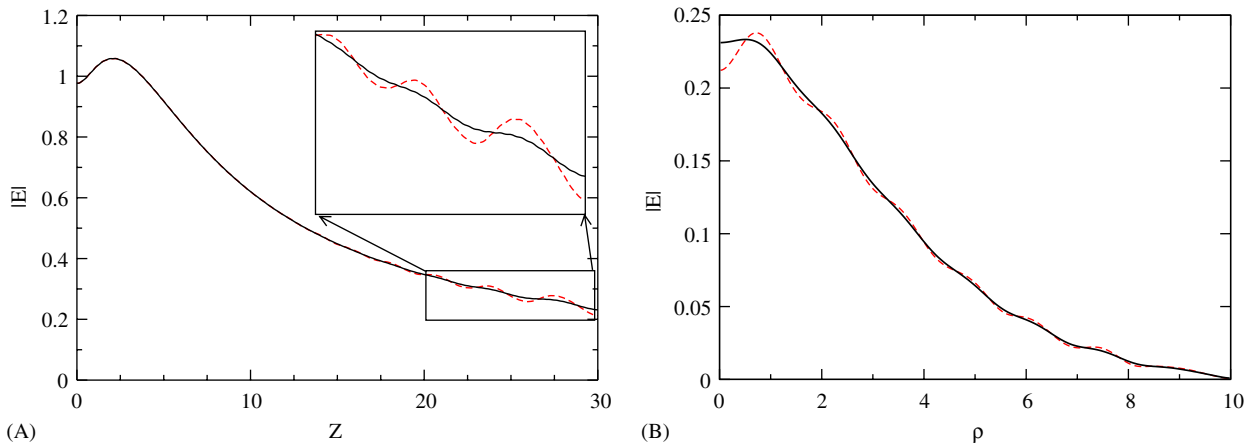
Fig. 3. Solution of the NLH (2) with $p = 0.7$ under the Dirichlet (dashed) and radiation (solid) transverse boundary conditions. (A) On-axis amplitude $|E(0, z)|$; and (B) transverse profile $|E(\rho, z_{\max})|$.
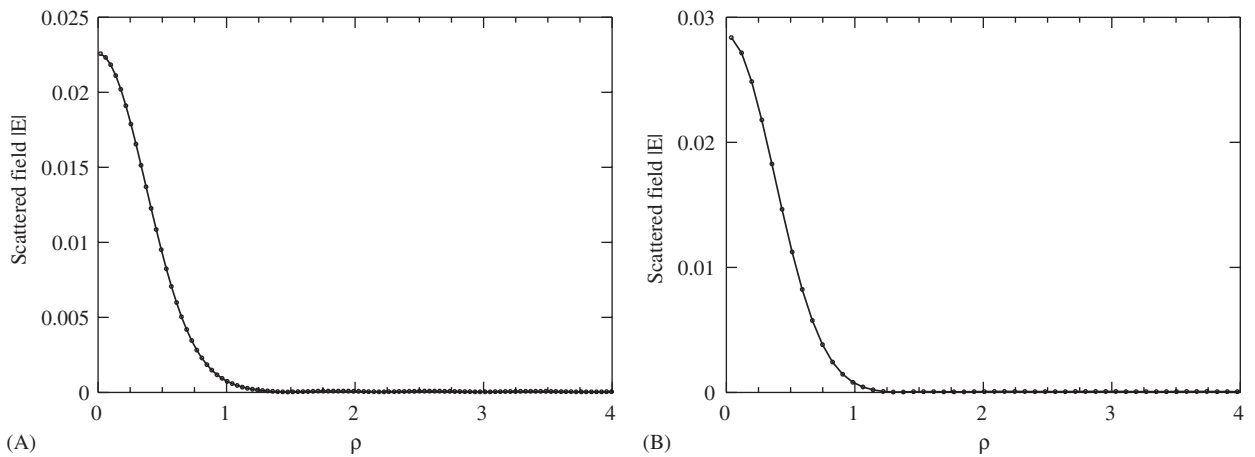

Fig. 4. Backscattered field $|E_{\text{scat}}(\rho, 0)|$. (A) $p = 0.7$; (B) $p = 0.97$.

Dirichlet boundary condition displays much larger fluctuations than the solution with the radiation boundary conditions (especially towards $z_{\max}$, see inset), due to the reflections from the artificial boundary $\rho = \rho_{\max}$. The amplitude in the transverse direction at $z_{\max}$, $|E(\rho, z_{\max})|$, see Fig. 3B, also shows that the Dirichlet boundary condition causes much larger fluctuations than the radiation boundary condition.

An important feature of our method is its capability to calculate the backscattered wave. Indeed, the difference $E(\rho, 0) - E_{\text{inc}}^{\text{left}}(\rho)$ is equal to the backscattered field at $z = 0$. It is plotted in Fig. 4A for $p = 0.7$. As expected, the backscattered field is small compared to the forward propagating wave, and the maximal backscattering is attained at $\rho = 0$. To the best of our knowledge, this is the first ever direct calculation of backscattering in a Kerr medium for the $3D$ physical setting.

For the computations presented in Fig. 5, we have increased the nonlinearity to $p = 0.97$ (i.e., to slightly below the threshold for collapse). The method did not converge for the Dirichlet boundary condition, but it did converge for the radiation transverse boundary condition. As expected for a stronger nonlinearity, the initial focusing is also much stronger, the diffraction is slower and the backscattered field at $z = 0$ is larger, see Fig. 4B.
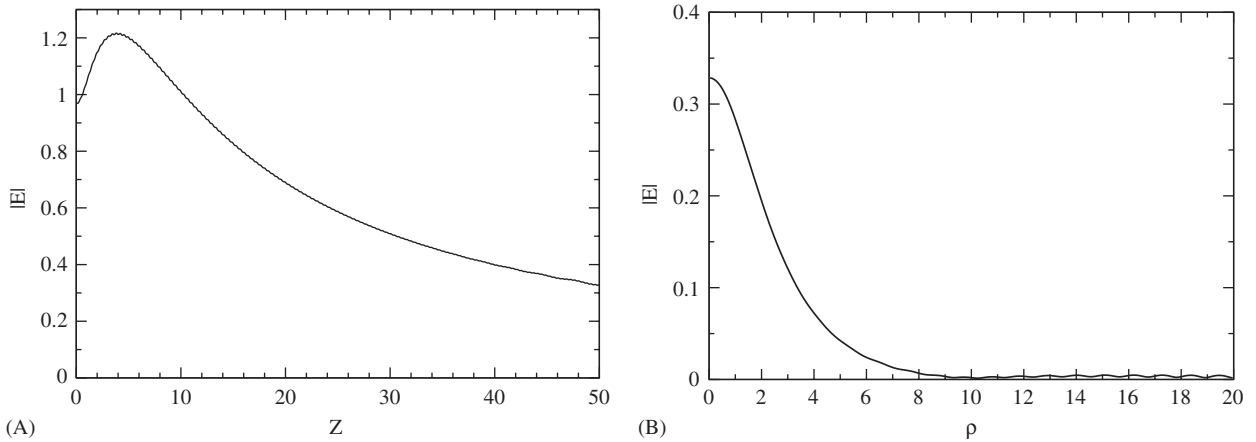
Fig. 5. Same as Fig. 3 for the radiation boundary condition, but with $p = 0.97$.

Table 3
Computational speedup ($T_{\mathrm{old}}/T_{\mathrm{new}}$) obtained by the Green-function based $1D$ solver

(h_ρ, h_z)	$\left(\frac{\lambda_0}{4}, \frac{\lambda_0}{10}\right)$	$\left(\frac{\lambda_0}{8}, \frac{\lambda_0}{20}\right)$
Total runtime speedup	2.5	2.41
$1D$ solver runtime speedup	10	9.6

4.4. Advantages of the convolution based 1D solver

In order to quantify the computational benefits from employing the one-dimensional convolution based solver described in Section 3.4, the full algorithm was used with the old LU decomposition based solver of [8,9], as well as with the new solver. The computations were conducted for two different grid resolutions, and the corresponding speedups (old execution time vs. new execution time) are presented in Table 3. We see that the direct implementation of convolutions with the discrete Green's function, as opposed to the LU factorization, brings along roughly an order of magnitude speedup for the $1D$ solver itself, which translates into a factor of 2.4 speedup for the overall computational procedure.

5. Discussion

In this paper, we introduced two major changes to the algorithm developed in [8,9] for solving the NLH equation. The first one is a new technique employed in the framework of the separation of variables for integrating the one-dimensional Helmholtz equations subject to two-way boundary conditions. This approach has a number of important benefits. One does not need to explicitly build the longitudinal discretization matrix, and does not need to carry out its LU decomposition for each eigenmode before the iterations. Indeed, in our simulations, we obtained a very substantial reduction of the overall computational time with the help of the new approach.

The second major change is the extension of the algorithm to a three-dimensional axially symmetric setting. This allowed us to study the effect of nonparaxiality and backscattering on self-focusing of electromagnetic waves in the genuine physical case (three space dimensions and a cubic nonlinearity). Studies of that kind have not been possible until now. The transition to a three-dimensional cylindrically symmetric setting necessitated a different implementation of the transverse discrete boundary conditions. In addition, since the fourth-order discrete transverse eigenvectors are not real orthogonal, the inverse of the transformation matrix that renders the separation of variables has to be calculated in a full-fledged way, unlike in the Cartesian cases, when it reduces to transposition. The additional computational cost for this matrix inversion is $\mathcal{O}(M^3)$ arithmetic operations, where M is the transverse dimension of the grid. Note that we

are typically interested in solving the NLH on "slim" computational domains, with the longitudinal size larger than the transverse size. On top of this, the longitudinal grid resolution is typically higher than the transverse grid resolution, which altogether results in the longitudinal dimension N being considerably larger than the transverse dimension M. On every iteration, i.e., many times altogether in the course of computation, we perform the separation of variables at a cost of $\mathcal{O}(N \cdot M^2)$ arithmetic operations. Consequently, the one-time $\mathcal{O}(M^3)$ cost of the matrix inversion is acceptable, and does not noticeably degrade the overall performance.

In the Cartesian case, implementation of the transverse local radiation boundary condition facilitated a very considerable reduction in the size of the computational domain, compared to the Dirichlet boundary conditions. However, the computational cost of the transformation by means of the matrix of eigenvectors was only $\mathcal{O}(M \log M)$ for the Dirichlet boundary conditions (with the help of FFT) and $\mathcal{O}(M^2)$ for the radiation boundary conditions. From this perspective the advantage of reducing the size of the domain could have been partially reversed by a higher transformation cost. In the three-dimensional axially symmetric setting, the advantage of the radiation condition is more apparent. Indeed, while it allows to set the transverse computation boundary much closer to the center of the domain, the forward and backward transformations are $\mathcal{O}(M^2)$ for both the Dirichlet and the radiation conditions.

References

[1] M.S. Agranovich, B.Z. Katsenelenbaum, A.N. Sivov, N.N. Voitovich, Generalized Method of Eigenoscillations in Diffraction Theory, Wiley-VCH Verlag Berlin GmbH, Berlin, 1999 (translated from the Russian manuscript by Vladimir Nazaikinskii).

[2] N. Akhmediev, A. Ankievicz, J. Soto-Crespo, Does the nonlinear Schrödinger equation correctly describe beam propogation?, Opt. Lett. 18 (1993) 411.

[3] M. Feit, J. Fleck, Beam nonparaxiality, filament formation and beam breakup in the self-focusing of optical beams, J. Opt. Soc. Amer. B 5 (1988) 633.

[4] G. Fibich, B. Ilan, Self focusing of elliptic beams: an example of the failure of the aberrationless approximation, J. Opt. Soc. Amer. B 17 (2000) 1749–1758.

[5] G. Fibich, B. Ilan, S.V. Tsynkov, Computation of nonlinear backscattering using a high-order numerical method, J. Sci. Comput. 17 (1–4) (2002) 351–364.

[6] G. Fibich, B. Ilan, S.V. Tsynkov, Backscattering and nonparaxiality arrest collapse of damped linear waves, SIAM J. Appl. Math. 63 (5) (2003) 1718–1736.

[7] G. Fibich, G.C. Papanicolaou, Self-focusing in the perturbed and unperturbed nonlinear Schrödinger equation in critical dimension, SIAM J. Appl. Math. 60 (1999) 183–240.

[8] G. Fibich, S. Tsynkov, High-order two-way artificial boundary conditions for nonlinear wave propagation with backscattering, J. Comput. Phys. 171 (2001) 632–677.

[9] G. Fibich, S. Tsynkov, Numerical solution of the nonlinear Helmholtz equation using nonorthogonal expansions, J. Comput. Phys. 210 (2005) 183–224.

[10] I. Harari, E. Turkel, Accurate finite difference methods for time-harmonic wave propagation, J. Comput. Phys. 119 (2) (1995) 252–270.

[11] J. Lončarić, S.V. Tsynkov, Optimization of acoustic source strength in the problems of active noise control, SIAM J. Appl. Math. 63 (4) (2003) 1141–1183.

[12] A.K.D. Moll, G. Fibich, Self-similar optical wave collapse: observation of the Townes profile, Phys. Rev. Lett. 90 (2003) 203902.

[13] A. Newell, J. Moloney, Nonlinear Optics, Addison-Wessley, Reading, MA, 1992.

[14] V.S. Ryaben'kii, Necessary and sufficient conditions for good definition of boundary value problems for systems of ordinary difference equations, U.S.S.R. Comput. Math. and Math. Phys. 4 (1964) 43–61.

[15] I. Singer, E. Turkel, High-order finite difference methods for the Helmholtz equation, Comput. Methods Appl. Mech. Eng. 163 (1–4) (1998) 343–358.

[16] I. Singer, E. Turkel, A perfectly matched layer for the Helmholtz equation in a semi-infinite strip, J. Comput. Phys. 201 (2) (2004) 439–465.

[17] W. Strauss, Nonlinear Wave Equations, American Mathematical Society, 1989.

[18] C. Sulem, P.-L. Sulem, The Nonlinear Schrodinger Equation, Springer, Berlin, 1999.

[19] S.V. Tsynkov, Numerical solution of problems on unbounded domains. A review, Appl. Numer. Math. 27 (1998) 465–632.